
Fully Decoupled Neural Network Learning Using Delayed Gradients

Huiping Zhuang, Yi Wang, Qinglai Liu, Zhiping Lin

School of Electrical and Electronic Engineering

Nanyang Technological University, Singapore

{HUIPING001,WANG1241}@e.ntu.edu.sg, {liuql,EZPLIN}@ntu.edu.sg

Abstract

Using the back-propagation (BP) to train neural networks requires a sequential passing of the activations and the gradients, which forces the network modules to work in a synchronous fashion. This has been recognized as the lockings (i.e., the forward, backward and update lockings) inherited from the BP. In this paper, we propose a fully decoupled training scheme using delayed gradients (FDG) to break all these lockings. The proposed method splits a neural network into multiple modules that are trained independently and asynchronously in different GPUs. We also introduce a gradient shrinking process to reduce the stale gradient effect caused by the delayed gradients. In addition, we prove that the proposed FDG algorithm guarantees a statistical convergence during training. Experiments are conducted by training deep convolutional neural networks to perform classification tasks on benchmark datasets. The proposed FDG is able to train very deep networks (>100 layers) and very large networks (>35 million parameters) with significant speed gains while outperforming the state-of-the-art methods and the standard BP.

1 Introduction

In recent years, deep neural networks, e.g., convolutional neural network (CNN) [15] and recurrent neural network [8, 4], have demonstrated great success in numerous highly complex tasks. Such success is built, to a great extent, on the ability to train extremely deep networks enabled by ResNet [7] or other techniques with skip-connection-like structures [25, 24, 9, 6]. Training networks with back-propagation (BP) [22] is a standard practice but it requires a complete forward and backward pass before the parameter update can be finished. This easily leads to inefficiency especially for training deeper networks, which is recognized as the lockings [12] (i.e., forward, backward and update lockings) inherited from the standard BP. The existence of these lockings keeps the majority of the network on hold during the training, thereby compromising the efficiency.

In order to improve the efficiency, there have been a number of contributions of decoupling the training by splitting the network into multiple modules to facilitate model parallelization. These techniques can be roughly categorized into two groups: the backward-unlocking (BU) methods and the local error learning (LEL) methods.

The BU-based methods have access to the global information from the top layer and could break the backward locking. An additional benefit is that they often introduce no extra trainable parameters while enabling decoupling behaviors. Nonetheless, a full forward pass is still required in advance of any parameter update. One important motivation for these techniques is to promote biological plausibility, which focuses on removing the weight symmetry and the gradient propagation from the BP. Feedback alignment (FA) [17] removes the weight symmetry by replacing symmetrical weights with random ones. Direct feedback alignment [19] following the FA replaces the BP by unlocking the backward pass and enables a simultaneous update for all layers. However, these biologically

Table 1: Comparison with state-of-the-art methods in terms of lockings and extra trainable parameters.

Methods	DDG [11]	DNI [12]	DGL [2]	FDG (ours)
Any Lockings	Yes	No	No	No
Extra trainable parameters	No	Yes	Yes	No

inspired approaches suffer from performance losses and are shown to scale poorly on more complex datasets [1]. On the other hand, the *delayed gradients* provide another solution of breaking the backward pass. The recently proposed decoupled learning using delayed gradients (DDG) [11] is able to train extremely deep (up to 110 layers) CNNs and shows no performance loss in certain cases while reducing the training time. Since the DDG is still constrained by the forward locking, the computation time could only be reduced by about 50% even with multiple GPUs.

The LEL-based methods use the local information and are more promising in terms of decoupling ability. This is because they are able to fully decouple (breaking the forward, backward and update lockings) the neural network training. The full decoupling is achieved by building auxiliary local loss functions to generate local error gradients, severing the gradient flow between the adjacent modules. The decoupled neural interface (DNI) proposed in [12] is one of the pioneers exhibiting parallel training potential for neural networks. This technique uses a local neural network to generate synthetic error gradients for the hidden layers so that the update could happen before completing either the forward or the backward pass. However, the DNI has been shown less capable of learning well and even exhibiting convergence problems in deeper networks [11]. In [18], local classifiers with cross-entropy loss are adopted showing potentials to train the hidden layers simultaneously. It has been shown that the local classifier alone fails to match the performance of a standard BP. In [20], a similarity measure combined with the local classifier is introduced to provide local error gradients. The mixed loss functions can produce classification performances comparable with or even better than the BP baselines but are currently tested only in VGG-like networks (≤ 13 layers). Very recently, the depth problem of the LEL-based methods is alleviated by decoupled greedy learning (DGL) [2], which is able to train extremely deep networks (≥ 100 layers) while maintaining comparable performance against a standard BP. The common sacrifice that any LEL technique has to make is the introduction of extra trainable parameters imposed by auxiliary networks. For instance, to match the standard BP, the local learning in [20] needs to train several times more parameters.

In summary, both BU-based and LEL-based methods can decouple the training of neural networks while obtaining comparable performances against the standard BP. In comparison, LEL-based methods lead in fully decoupling the network learning but introduce extra trainable parameters. The BU-based methods behave in the opposite way. In this paper, we propose a fully decoupled training scheme using delayed gradients (FDG) sharing both merits of the BU-based and the LEL-based techniques (see Table 1). Although we adopt delayed gradients like the DDG [11] and other asynchronous SGD methods [5, 16, 26], the proposed FDG utilizes a different training scheme, which is more efficient and has better generalization ability. The main contributions of this work are as follows:

- We propose the FDG, a novel training technique that breaks the forward, backward and update lockings without introducing extra trainable parameters. We also develop a gradient shrinking (GS) process that can reduce the stale gradient effect caused by utilizing the delayed gradients.
- Theoretical analysis is provided showing that the proposed technique guarantees a statistical convergence under certain conditions.
- We conduct experiments by training deep CNNs and show that the proposed FDG obtains comparable or even better performances on benchmark datasets while reducing a significant amount of computation time.

2 Background

In this section, we provide some basic background knowledge for training a feedforward neural network. The forward, backward and update lockings are also revisited.

Assume we need to train an L -layer network. The l^{th} ($l \leq L$) layer produces an activation $\mathbf{z}_l = A_l(\mathbf{z}_{l-1}; \boldsymbol{\theta}_l)$ by taking \mathbf{z}_{l-1} as its input, where A_l is an activation function and $\boldsymbol{\theta}_l \in \mathbb{R}^{n_l}$ is a column vector representing the weights in layer l . The sequential generation of the activations constructs the *forward locking* [12] since \mathbf{z}_l will not be available before all the dependent activations are obtained. Let $\boldsymbol{\theta} = [\boldsymbol{\theta}_1^T, \boldsymbol{\theta}_2^T, \dots, \boldsymbol{\theta}_L^T]^T \in \mathbb{R}^{\sum_{i=1}^L n_i}$ denote the parameter vector of the network. Assume f is a loss function that maps a high-dimensional vector to a scalar. The learning of the feedforward network can then be summarized as the following optimization problem:

$$\underset{\boldsymbol{\theta} = [\boldsymbol{\theta}_1^T, \boldsymbol{\theta}_2^T, \dots, \boldsymbol{\theta}_L^T]^T}{\text{minimize}} \quad f_{\mathbf{x}}(\boldsymbol{\theta}) \quad (1)$$

where \mathbf{x} represents the input-label information (or training samples). We will drop the \mathbf{x} in (1) in this paper for convenience: $f_{\mathbf{x}}(\boldsymbol{\theta}) \rightarrow f(\boldsymbol{\theta})$.

The gradient descent algorithm is often used to solve (1) by updating the parameter $\boldsymbol{\theta}$ iteratively. At iteration t , we have

$$\boldsymbol{\theta}^{t+1} = \boldsymbol{\theta}^t - \gamma_t \mathbf{g}^t \text{ or, } \boldsymbol{\theta}_l^{t+1} = \boldsymbol{\theta}_l^t - \gamma_t \mathbf{g}_l^t, \quad l = 1, \dots, L \quad (2)$$

where γ_t is the learning rate and $\mathbf{g}^t = [(\mathbf{g}_1^t)^T, (\mathbf{g}_2^t)^T, \dots, (\mathbf{g}_L^t)^T]^T \in \mathbb{R}^{\sum_{i=1}^L n_i}$ is the gradient vector obtained by $\mathbf{g}_l^t = \nabla f(\boldsymbol{\theta}_l^t) = \frac{\partial f(\boldsymbol{\theta}_l^t)}{\partial \boldsymbol{\theta}_l^t}$. If the training sample size is large, we apply stochastic gradient descent (SGD) as a replacement by obtaining the gradient vector with respect to $f_{\mathbf{x}^t}(\boldsymbol{\theta}^t)$ where \mathbf{x}^t is a mini-batch of \mathbf{x} . Such a replacement is based on the following realistic assumption:

$$\mathbb{E}\left[\frac{\partial f_{\mathbf{x}^t}(\boldsymbol{\theta}^t)}{\partial \boldsymbol{\theta}_l^t}\right] = \frac{\partial f_{\mathbf{x}}(\boldsymbol{\theta}^t)}{\partial \boldsymbol{\theta}_l^t} \text{ or, } \mathbb{E}\left[\nabla f_{\mathbf{x}^t}(\boldsymbol{\theta}_l^t)\right] = \nabla f(\boldsymbol{\theta}_l^t). \quad (3)$$

To obtain the gradient vectors, the BP (also known as the chain rule) can be employed. One could calculate the gradients in layer l from the gradients in layer j ($j > l$):

$$\mathbf{g}_l^t = \frac{\partial f_{\mathbf{x}^t}(\boldsymbol{\theta}^t)}{\partial \boldsymbol{\theta}_l^t} = \frac{\partial \boldsymbol{\theta}_j^t}{\partial \boldsymbol{\theta}_l^t} \frac{\partial f_{\mathbf{x}^t}(\boldsymbol{\theta}^t)}{\partial \boldsymbol{\theta}_j^t} = \frac{\partial \boldsymbol{\theta}_j^t}{\partial \boldsymbol{\theta}_l^t} \mathbf{g}_j^t \quad (4)$$

which also indicates a dependency of \mathbf{g}_l^t on \mathbf{g}_j^t . In other words, the gradients in layer l would remain unavailable until the gradient computations of all the dependent layers are completed. This is also known as the *backward locking* [12] in BP. The existence of this locking prevents the update of $\boldsymbol{\theta}_l^t$ before $\boldsymbol{\theta}_j^t$. In addition, the parameter update must come after executing the forward pass. This is recognized as the *update locking* [12]. In the following, we will show that a full decoupling (including breaking the forward, backward and update lockings) can be achieved.

3 Fully Coupled Neural Network Learning

In this section, we give details of the proposed FDG. This technique provides a fully decoupled asynchronous learning algorithm with a gradient shrinking (GS) process that is able to reduce the accuracy loss caused by the delayed gradients.

3.1 The Proposed FDG

We first split the network into K modules with each module containing a stack of layers. Then we rewrite $\boldsymbol{\theta}^t, \mathbf{g}^t$ in terms of modules as

$$\boldsymbol{\theta}^t = [(\boldsymbol{\theta}_{q(1)}^t)^T, \dots, (\boldsymbol{\theta}_{q(K)}^t)^T]^T, \quad \mathbf{g}^t = [(\mathbf{g}_{q(1)}^t)^T, \dots, (\mathbf{g}_{q(K)}^t)^T]^T$$

$$\boldsymbol{\theta}_{q(k)}^t = [(\boldsymbol{\theta}_{m_k}^t)^T, \dots, (\boldsymbol{\theta}_{m_{k+1}-1}^t)^T]^T, \quad \mathbf{g}_{q(k)}^t = [(\mathbf{g}_{m_k}^t)^T, \dots, (\mathbf{g}_{m_{k+1}-1}^t)^T]^T$$

where $q(k)$ denotes the layer indices in module k and m_k represents the first index in $q(k)$.

As illustrated in Figure 1(a), during the decoupled training, module k is able to perform BP using the delayed gradients passed from module $k+1$. Also, the error gradients in the first layer are passed to module $k-1$, while the activations of the last layer are passed to module $k+1$. This can be summarized as the following steps for module k ($k < K$):

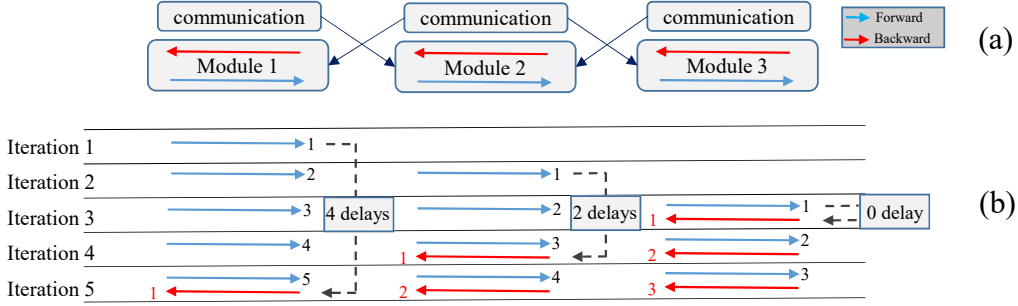


Figure 1: The proposed FDG: an example with 3 split modules. (a) the backward, forward and communication steps for the modules. (b) a pipeline-like parallel training scheme for the proposed FDG. We can observe that there is a delay of $2(K - k)$ of gradients from the last module to module k .

- **backward:** after receiving the delayed error gradients $\hat{g}_{m_{k+1}}^{t-2}$ from module $k + 1$, we run BP to compute the gradients for each layer: $\hat{g}_l^t = \frac{\partial \theta_{m_{k+1}}}{\partial \theta_l} \hat{g}_{m_{k+1}}^{t-2}$, and then update the module through

$$\theta_l^{t+1} = \theta_l^t - \gamma_t \hat{g}_l^t. \quad (5)$$

After that, we save error gradients in the first layer $\hat{g}_{m_k}^t$ for communication.

- **forward:** run the input through this module and save the activation $z_{m_{k+1}-1}^t$ for communication.

- **communication:** pass the saved stale error gradients $\hat{g}_{m_k}^t$ to module $k - 1$ and pass the saved activation $z_{m_{k+1}-1}^t$ to module $k + 1$ as its new input.

In particular, at iteration t , \hat{g}_l^t can be further explored such that

$$\hat{g}_l^t = \frac{\partial \theta_{m_{k+1}}}{\partial \theta_l} \hat{g}_{m_{k+1}}^{t-2} = \frac{\partial \theta_{m_{k+1}}}{\partial \theta_l} \frac{\partial \theta_{m_{k+2}}}{\partial \theta_{m_{k+1}}} \hat{g}_{m_{k+1}}^{t-4} = \frac{\partial \theta_{m_{k+1}}}{\partial \theta_l} \cdots \frac{\partial \theta_{m_K}}{\partial \theta_{m_{K-1}}} \hat{g}_{m_K}^{t-2(K-k)} = g_l^{d_{K,k}(t)} \quad (6)$$

where $d_{K,k}(t) = t - 2(K - k)$ indicating that there is a delay of $2(K - k)$ of gradients from module K to module k (see Figure 1(b)). In module K , no delay is expected because it interacts with the label information directly. It is easily noticed that the backward, forward and communication steps break the forward and the backward lockings since all the modules can be trained in parallel as shown in Figure 1(b).

On the other hand, different from the traditional training strategy which forwards the input before backwarding the error gradients, we do the backward pass first and update the module before producing the module output. This update-before-forward strategy also breaks the update locking.

3.2 The Gradient Shrinking Process

Using the delayed gradients enables model parallelization but could also lead to certain performance loss. This is a common phenomenon observed in algorithms with stale gradients [3]. To compensate the performance loss, we introduce a gradient shrinking (GS) process before back-propagating the delayed error gradients through each module.

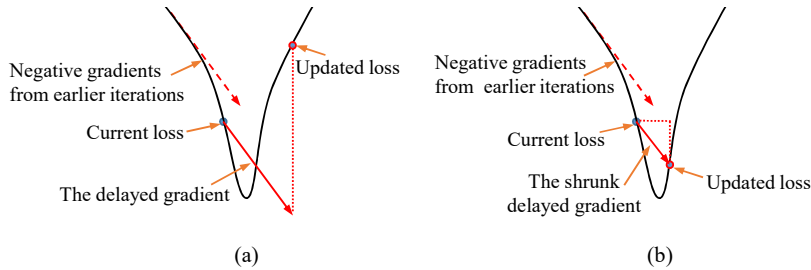


Figure 2: An intuitive interpretation of the benefit brought by the GS process.

The GS process works in a very straightforward manner. At iteration t , before backwarding the delayed error gradients through module k , we shrink the error gradients by multiplying it with a shrinking factor β ($0 < \beta \leq 1$). This can be shown by rewriting \hat{g}_l^t as

$$\hat{g}_l^t = \beta^{K-k} g_l^{d_{K,k}(t)}. \quad (7)$$

Then the module is updated through (5). In particular, if $\beta = 1$, the GS process is not used.

The GS process works similarly by scaling the learning rate in the corresponding module, determining how much we should move towards the direction of the negative gradients. We can interpret this process in an intuitive way shown in Figure 2. The delayed error gradients, especially with longer delays, would lead to deteriorated performance [3]. Figure 2(a) shows a scenario where the delayed gradients cause the learning to miss the local minimum to a large margin. By using the shrunk delayed gradients, we could have better chances of reducing the stale gradient effect (see Figure 2(b) for an illustration). The proposed FDG with the GS process is summarized in Algorithm I with SGD optimizer.

Comparison to DDG [11]: Although the DDG also adopts the delayed gradients, we have shown that the proposed FDG breaks all the lockings while the DDG only succeeds in unlocking the backward pass. Additionally, the GS process is proposed to process the delayed gradients while the DDG feeds them directly to the modules. The effectiveness of the GS process will be illustrated in experiments.

Algorithm I: FDG (SGD)

Required: learning rate γ_t , number of split modules K , gradient shrinking factor β .

- Split the network into K modules and initialize them with $\theta_{q(1)}^0, \dots, \theta_{q(K)}^0$.

for $t = 0, 1, 2, \dots, T - 1$:

Parallel for $k = 1, \dots, K$, do (**backward** and **forward**):

- **if** not the last module:

- compute the shrunk delayed gradients in each layer: $\hat{g}_l^t = \beta \frac{\partial \theta_{m_{k+1}}}{\partial \theta_l} \hat{g}_{m_{k+1}}^{t-2}$.
- update the module: $\theta_l^{t+1} = \theta_l^t - \gamma_t \hat{g}_l^t$; save the error gradients of the first layer $\hat{g}_{m_k}^t$.
- forward the input through module k ; produce and save the activation $z_{m_{k+1}-1}^t$.

- **else**:

- update the module (without delay).
- forward the input through module, calculating the loss.
- do BP for the module with respect to the loss; save the error gradients of the first layer $g_{m_K}^t$.

for $k = 2, \dots, K$, do (**communication**):

- clone the activation of module $k - 1$ as the input of module k .

- clone the error gradients of the first layer in module k as the delayed gradients of module $k - 1$.

4 Convergence Analysis

In this section, we prove that the proposed FDG in Algorithm I guarantees a statistical convergence. This proof is mainly based on two commonly used assumptions as follows.

Assumption 1. *The gradient of the loss function $f(\theta)$ is Lipschitz continuous. This means there*

exists a constant $L > 0$ such that $\forall \theta, \eta \in \mathbb{R}^{i=1} \sum_{i=1}^L n_i$ and $\forall \theta_{q(k)}, \eta_{q(k)} \in \mathbb{R}^{\sum_{j=m_k}^{m_{k+1}-1} n_j}$:

$$\|\nabla f(\theta) - \nabla f(\eta)\|_2 \leq L \|\theta - \eta\|_2 \quad (8)$$

$$\|\nabla f(\theta_{q(k)}) - \nabla f(\eta_{q(k)})\|_2 \leq L \|\theta_{q(k)} - \eta_{q(k)}\|_2. \quad (9)$$

Assumption 2. *The second moment of the stochastic gradient is bounded. This means there exists a constant $M \geq 0$ such that:*

$$\|\nabla f_{\mathbf{x}_t}(\theta)\|_2^2 \leq M. \quad (10)$$

Under Assumptions 1 and 2, we can obtain the FDG's convergence property that is similar to the DDG's [11] in the following theorem.

Theorem 1. Let Assumptions 1 and 2 hold. Assume that the learning rate is diminishing and $L\gamma_t \leq 1$. The proposed FDG in Algorithm I satisfies

$$E[f(\boldsymbol{\theta}^{t+1})] - f(\boldsymbol{\theta}^t) \leq -\frac{\gamma_t}{2} Z_1 + \gamma_t^2 Z_2 \quad (11)$$

where

$$\begin{aligned} Z_1 &= \sum_{k=1}^K \beta^{K-k} \|\nabla f(\boldsymbol{\theta}_{q(k)}^t)\|_2^2 \\ Z_2 &= LM \frac{\beta^K - 1}{\beta - 1} + LM \sum_{k=1}^K \beta^{3(K-k)} (t - \max\{0, d_{K,k}(t)\}). \end{aligned}$$

As shown in Theorem 1, the behavior of the expected loss value $E[f(\boldsymbol{\theta}^{t+1})]$ is controlled by the learning rate γ_t . If the right side of (11) is less than zero, i.e.,

$$-\frac{\gamma_t}{2} Z_1 + \gamma_t^2 Z_2 \leq 0 \Rightarrow \gamma_t \leq \min\left\{\frac{1}{L}, \frac{Z_1}{2Z_2}\right\},$$

the FDG guarantees convergence statistically. The proof of Theorem 1 is provided in the supplementary materials.

5 Experiments

In this section, we conduct experiments with several ResNet-like structures on image classification tasks (on CIFAR-10 and CIFAR-100 [14] datasets). The conducted experiments show that the proposed FDG is able to obtain comparable or better results against the state-of-the-art methods and the BP baselines while accelerating the training significantly. The source code and trained models will be publicly available¹.

Implementation Details: We implement our proposed method in Pytorch platform [21], and evaluate it using ResNet [7] and WRN [25] models on CIFAR-10 and CIFAR-100 [14]. These datasets are pre-processed with standard data augmentation (i.e., random cropping, random horizontal flip and normalizing [7, 9]). We use SGD optimizer with an initial learning rate of 0.1. The momentum and weight decay are set as 0.9 and 5×10^{-4} respectively. All the models are trained using a batch size of 128 for 300 epochs. The learning rate is divided by 10 at 150, 225 and 275 epochs. Our experiments are run using one or more Tesla K80 GPUs. The test errors of the FDG are reported by the median of 3 runs.

Table 2: The Top 1 errors for various CNN structures on CIFAR-10 dataset under a split number $K=2$. “-” indicates that the results are not reported in the original paper. Results with “*” are rerun using our training strategy. We use $\gamma_t = 0.01$ to warm up the training of ResNet-110 for 3 epochs.

Architecture	# params	BP	DDG [11]	DGL [2]	FDG
ResNet-20	0.27M	8.75%[7]/7.78%*	-	-	7.92%($\beta=1$)/ 7.23% ($\beta=0.2$)
ResNet-56	0.46M	6.97%[7]/6.19%*	6.89%	-	6.20%($\beta=1$)/ 5.90% ($\beta=0.5$)
ResNet-110	1.70M	6.41%[7]/5.79%*	6.59%	6.50 \pm 0.10%	5.79%($\beta=1$)/ 5.73% ($\beta=0.5$)
ResNet-18	11.2M	6.48%[10]/4.87%*	-	-	4.82%($\beta=1$)/ 4.79% ($\beta=0.8$)
WRN-28-10	36.5M	4.00%[25]	-	-	4.13%($\beta=1$)/ 3.85% ($\beta=0.7$)

5.1 Compare with BP and State-of-the-Art Methods

We compare performances of four different methods, including the BP, the DDG [11], the DGL [2] and our proposed FDG. The DNI [12] is not included as its performance deteriorates severely with deeper networks [11].

CIFAR-10: We begin by reporting the classification results on the CIFAR-10 dataset, which includes 50000 training and 10000 testing color images with 10 classes. The networks are trained using 50000 training samples without any validation and we report the test error at the last epoch.

¹<https://github.com/ZHUANGHP/FDG.git>

Table 3: The Top 1 errors for various CNN structures on CIFAR-100 dataset under a split number $K=2$. “-” indicates that the results are not reported in the original paper. Results with “*” are rerun using our training strategy. We use $\gamma_t = 0.01$ to warm up the training of ResNet-110 for 3 epochs.

Architecture	# params	BP	DDG [11]	FDG
ResNet-56	0.46M	30.21%[11]/ 27.68%*	29.83%	27.87%($\beta=1$)/27.70%($\beta=0.8$)
ResNet-110	1.70M	28.10%[11]/25.82%*	28.61%	25.73%($\beta=1$)/ 25.43%($\beta=0.5$)
ResNet-18	11.2M	22.35%*	-	22.78%($\beta=1$)/ 22.18%($\beta=0.5$)
WRN-28-10	36.5M	19.2%[25]	-	20.28%($\beta=1$)/ 19.08%($\beta=0.6$)

In this CIFAR-10 experiment, we split the original network roughly at the center into two modules ($K=2$) and train them asynchronously and independently in 2 GPUs. In the conventional ResNet structures, we rerun the BP baselines in [7] using our training strategy, which gives better results than those reported in [11] and [2]. Since we use SGD instead of Adam [13] in the experiments, the improved baselines might be because the adaptive optimizers (e.g., Adam) are more prone to over-fitting [23].

The corresponding classification results are reported in Table 2. We can observe that our proposed method is able to achieve lower classification errors than all the state-of-the-art methods. The proposed FDG is validated by reporting the individual results with and without the GS process. By shrinking the delayed error gradients, the generalization abilities of these ResNet-like networks are enhanced to even surpass their BP counterparts. In particular, the improvements in ResNet-20 and WRN-28-10 are not trivial. The delayed gradients can be treated as the up-to-date gradients with noises. This poses difficulties for the networks to learn, but it also introduces certain regularization during training, which explains the improved performances. We also provide the learning curves (see the top panel in Figure 3) for ResNet-56 and ResNet-110. It is clear that our proposed method is able to converge in the same way a standard BP does throughout the training process. In particular, the error rate of 3.85% by decoupling the WRN-28-10 is a new state-of-the-art result for the CIFAR-10 among the published decoupling techniques.

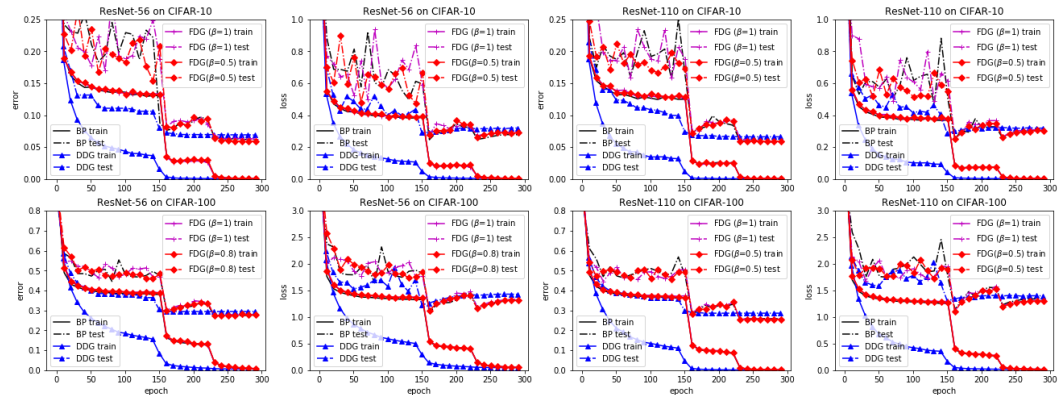


Figure 3: Learning curves of the BP, the DDG and the FDG for ResNet-56 and ResNet-110 on CIFAR-10 and CIFAR-100 datasets. The top panel indicates the learning curves (on error and loss) on CIFAR-10. The bottom panel shows the learning curves on CIFAR-100.

CIFAR-100: We now study the classification performance ($K=2$) on CIFAR-100, which contains the same number of training and testing samples as CIFAR-10 but with 100 classes. The training strategy follows the CIFAR-10 experiment and the performance is reported by the Top 1 error rate.

We also rerun the baselines using our training strategy, which again overtake the baselines provided in [11]. The classification results are reported in Table 2. We observe that the proposed FDG again beats the state-of-the-art methods by improving their classification performances by at least 2%. More importantly, the classification performances of the proposed FDG are able to match the rerun BP baselines. The learning curves shown in the bottom panel of Figure 3 indicate the proposed

method converges in the same way as the standard BP. The Top 1 error rate of 19.08% is also a new state-of-the-art result for the CIFAR-100 dataset among the published decoupling methods.

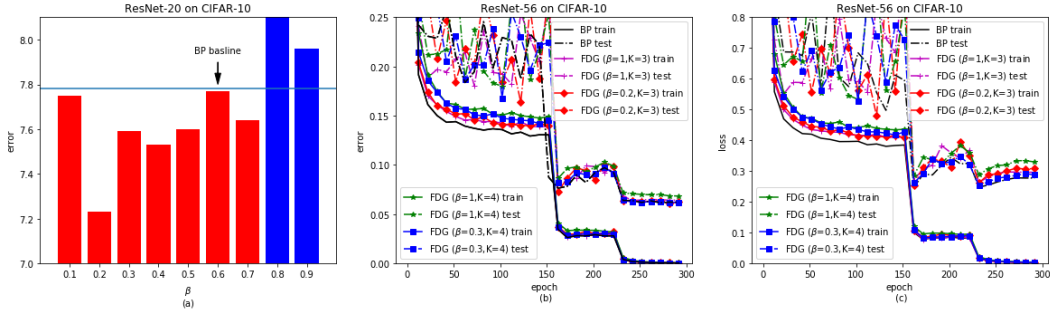


Figure 4: (a) The impact of the GS process with different β for training ResNet-20 on CIFAR-10 dataset. The classification results that surpass the standard BP are painted red. (b)-(c) are the learning curves (on error and loss respectively) for ResNet-56 on CIFAR-10 by scaling to more GPUs.

5.2 The Impact of the GS Process

We empirically evaluate the impact of the GS process by experimenting with various values of the shrinking factor β . This evaluation is conducted by training the ResNet-20 on CIFAR-10 dataset. The bar chart in Figure 4(a) reports the Top 1 error rates. We notice that the results for the proposed FDG are able to surpass the BP baseline with a small effort of tuning the β . This also shows that the introduction of the GS process does enhance a network’s generalization ability.

5.3 Speed Gains for Scaling to More GPUs

In this experiment, we study the performance of ResNet-56 on CIFAR-10 by splitting it into $K=3$ and $K=4$ modules with each module trained in an independent GPU. The conducted experiment is to show the empirical behaviors of the proposed FDG in presence of more split modules. The results are shown in Table 4 where we list the test errors of FDG with $K = 2, 3, 4$ against the BP. It becomes more obvious that more split modules have caused the FDG to lose accuracy. By enforcing the GS process, the classification performances can be restored to the BP baselines. The improved performances indicate that the GS process plays an essential role in reducing the stale gradient effect especially with more split modules. Table 4 also shows that the use of more GPUs significantly reduces the computation time by more than 55%². On the other hand, as indicated in Figure 4(b)-(c), the convergence behaviors of the FDG with $K = 3, 4$ still exhibit little difference from the BP.

Table 4: The Top 1 errors and the computation time in percentage for training ResNet-56 on CIFAR-10 by scaling to more GPUs. We use $\gamma_t = 0.01$ to warm up the training ($K=3,4$) for 3 epochs.

Method	Test error	Time
BP	6.19%	100%
FDG($K=2$)	6.20%($\beta=1$)/ 5.90% ($\beta=0.5$)	60.64%
FDG($K=3$)	6.40%($\beta=1$)/ 6.08% ($\beta=0.2$)	52.03%
FDG($K=4$)	6.83%($\beta=1$)/ 6.14% ($\beta=0.3$)	44.32%

6 Conclusion

In this paper, we utilize the delayed gradients to develop a novel training technique FDG that is able to break the forward, backward and update lockings for neural network learning. We have also introduced the gradient shrinking process that can help reduce the stale gradient effect caused by the delayed gradients. In addition, theoretical analysis has shown that the proposed FDG guarantees

²One could obtain more significant acceleration by improving the efficiency of the communication among GPUs, but this is beyond the scope of this work.

a statistical convergence under certain conditions. Finally, we conduct experiments on CNNs, showing that the FDG outperforms the state-of-the-art methods and obtains comparable or even better performances against the standard BP while significantly accelerating the training process.

References

- [1] Sergey Bartunov, Adam Santoro, Blake Richards, Luke Marris, Geoffrey E Hinton, and Timothy Lillicrap. Assessing the scalability of biologically-motivated deep learning algorithms and architectures. In *Advances in Neural Information Processing Systems*, pages 9368–9378, 2018.
- [2] Eugene Belilovsky, Michael Eickenberg, and Edouard Oyallon. Decoupled greedy learning of CNNs. *arXiv preprint arXiv:1901.08164*, 2019.
- [3] Jianmin Chen, Xinghao Pan, Rajat Monga, Samy Bengio, and Rafal Jozefowicz. Revisiting distributed synchronous sgd. *arXiv preprint arXiv:1604.00981*, 2016.
- [4] Kyunghyun Cho, Bart Van Merriënboer, Caglar Gulcehre, Dzmitry Bahdanau, Fethi Bougares, Holger Schwenk, and Yoshua Bengio. Learning phrase representations using RNN encoder–decoder for statistical machine translation. *arXiv preprint arXiv:1406.1078*, 2014.
- [5] Jeffrey Dean, Greg Corrado, Rajat Monga, Kai Chen, Matthieu Devin, Mark Mao, Andrew Senior, Paul Tucker, Ke Yang, Quoc V Le, et al. Large scale distributed deep networks. In *Advances in neural information processing systems*, pages 1223–1231, 2012.
- [6] Xavier Gastaldi. Shake-shake regularization. *arXiv preprint arXiv:1705.07485*, 2017.
- [7] Kaiming He, Xiangyu Zhang, Shaoqing Ren, and Jian Sun. Deep residual learning for image recognition. In *Proceedings of the IEEE conference on computer vision and pattern recognition*, pages 770–778, 2016.
- [8] Sepp Hochreiter and Jürgen Schmidhuber. Long short-term memory. *Neural computation*, 9(8):1735–1780, 1997.
- [9] Gao Huang, Zhuang Liu, Laurens Van Der Maaten, and Kilian Q Weinberger. Densely connected convolutional networks. In *Proceedings of the IEEE conference on computer vision and pattern recognition*, pages 4700–4708, 2017.
- [10] Qiangui Huang, Kevin Zhou, Suya You, and Ulrich Neumann. Learning to prune filters in convolutional neural networks. In *2018 IEEE Winter Conference on Applications of Computer Vision (WACV)*, pages 709–718. IEEE, 2018.
- [11] Zhouyuan Huo, Bin Gu, Heng Huang, et al. Decoupled parallel backpropagation with convergence guarantee. In *International Conference on Machine Learning*, pages 2103–2111, 2018.
- [12] Max Jaderberg, Wojciech Czarnecki, Simon Osindero, Oriol Vinyals, Alex Graves, David Silver, and Koray Kavukcuoglu. Decoupled neural interfaces using synthetic gradients. In *ICML*, 2016.
- [13] Diederik P Kingma and Jimmy Ba. Adam: A method for stochastic optimization. *arXiv preprint arXiv:1412.6980*, 2014.
- [14] Alex Krizhevsky and Geoffrey Hinton. Learning multiple layers of features from tiny images. Technical report, 2009.
- [15] Yann LeCun, Léon Bottou, Yoshua Bengio, Patrick Haffner, et al. Gradient-based learning applied to document recognition. *Proceedings of the IEEE*, 86(11):2278–2324, 1998.
- [16] Xiangru Lian, Yijun Huang, Yuncheng Li, and Ji Liu. Asynchronous parallel stochastic gradient for nonconvex optimization. In *Advances in Neural Information Processing Systems*, pages 2737–2745, 2015.
- [17] Timothy P Lillicrap, Daniel Cownden, Douglas B Tweed, and Colin J Akerman. Random synaptic feedback weights support error backpropagation for deep learning. *Nature communications*, 7:13276, 2016.

- [18] Hesham Mostafa, Vishwajith Ramesh, and Gert Cauwenberghs. Deep supervised learning using local errors. *Frontiers in neuroscience*, 12:608, 2018.
- [19] Arild Nøkland. Direct feedback alignment provides learning in deep neural networks. In *Advances in neural information processing systems*, pages 1037–1045, 2016.
- [20] Arild Nøkland and Lars Hiller Eidnes. Training neural networks with local error signals. *arXiv preprint arXiv:1901.06656*, 2019.
- [21] Adam Paszke, Sam Gross, Soumith Chintala, Gregory Chanan, Edward Yang, Zachary DeVito, Zeming Lin, Alban Desmaison, Luca Antiga, and Adam Lerer. Automatic differentiation in pytorch. 2017.
- [22] Paul Werbos. Beyond regression: New tools for prediction and analysis in the behavioral sciences. *Ph. D. dissertation, Harvard University*, 1974.
- [23] Ashia C Wilson, Rebecca Roelofs, Mitchell Stern, Nati Srebro, and Benjamin Recht. The marginal value of adaptive gradient methods in machine learning. In *Advances in Neural Information Processing Systems*, pages 4148–4158, 2017.
- [24] Saining Xie, Ross Girshick, Piotr Dollár, Zhuowen Tu, and Kaiming He. Aggregated residual transformations for deep neural networks. In *Proceedings of the IEEE conference on computer vision and pattern recognition*, pages 1492–1500, 2017.
- [25] Sergey Zagoruyko and Nikos Komodakis. Wide residual networks. *arXiv preprint arXiv:1605.07146*, 2016.
- [26] Shuxin Zheng, Qi Meng, Taifeng Wang, Wei Chen, Nenghai Yu, Zhi-Ming Ma, and Tie-Yan Liu. Asynchronous stochastic gradient descent with delay compensation. In *Proceedings of the 34th International Conference on Machine Learning-Volume 70*, pages 4120–4129. JMLR. org, 2017.

A. Proof to Theorem 1

Proof. According to Assumption 1, the following inequality holds:

$$f(\boldsymbol{\theta}^{t+1}) \leq f(\boldsymbol{\theta}^t) + \nabla f(\boldsymbol{\theta}^t)^T (\boldsymbol{\theta}^{t+1} - \boldsymbol{\theta}^t) + \frac{L}{2} \left\| \boldsymbol{\theta}^{t+1} - \boldsymbol{\theta}^t \right\|_2^2. \quad (\text{a})$$

Taking the expectation on both sides, we have

$$\begin{aligned} & \mathbb{E} \left[f(\boldsymbol{\theta}^{t+1}) \right] \\ & \leq f(\boldsymbol{\theta}^t) - \gamma_t \mathbb{E} \left[\sum_{k=1}^K \nabla f(\boldsymbol{\theta}_{q(k)}^t)^T \hat{\mathbf{g}}_{q(k)}^t \right] + \frac{L\gamma_t^2}{2} \mathbb{E} \left[\sum_{k=1}^K \left\| \hat{\mathbf{g}}_{q(k)}^t \right\|_2^2 \right] \\ & = f(\boldsymbol{\theta}^t) - \gamma_t \mathbb{E} \left[\sum_{k=1}^K \beta^{K-k} \nabla f(\boldsymbol{\theta}_{q(k)}^t)^T \nabla f_{\mathbf{x}_{d_{K,k}(t)}}(\boldsymbol{\theta}_{q(k)}^{d_{K,k}(t)}) \right] \\ & \quad + \frac{L\gamma_t^2}{2} \mathbb{E} \left[\sum_{k=1}^K \beta^{2(K-k)} \left\| \nabla f_{\mathbf{x}_{d_{K,k}(t)}}(\boldsymbol{\theta}_{q(k)}^{d_{K,k}(t)}) \right\|_2^2 \right] \\ & \leq f(\boldsymbol{\theta}^t) - \gamma_t \mathbb{E} \left[\sum_{k=1}^K \beta^{K-k} \nabla f(\boldsymbol{\theta}_{q(k)}^t)^T \nabla f_{\mathbf{x}_{d_{K,k}(t)}}(\boldsymbol{\theta}_{q(k)}^{d_{K,k}(t)}) \right] \\ & \quad + \frac{L\gamma_t^2}{2} \mathbb{E} \left[\sum_{k=1}^K \beta^{K-k} \left\| \nabla f_{\mathbf{x}_{d_{K,k}(t)}}(\boldsymbol{\theta}_{q(k)}^{d_{K,k}(t)}) \right\|_2^2 \right] \\ & = f(\boldsymbol{\theta}^t) - \gamma_t \mathbb{E} \left[\sum_{k=1}^K \beta^{K-k} \nabla f(\boldsymbol{\theta}_{q(k)}^t)^T \left(\nabla f_{\mathbf{x}_{d_{K,k}(t)}}(\boldsymbol{\theta}_{q(k)}^{d_{K,k}(t)}) - \nabla f(\boldsymbol{\theta}_{q(k)}^t) + \nabla f(\boldsymbol{\theta}_{q(k)}^t) \right) \right] \\ & \quad + \frac{L\gamma_t^2}{2} \mathbb{E} \left[\sum_{k=1}^K \beta^{K-k} \left\| \nabla f_{\mathbf{x}_{d_{K,k}(t)}}(\boldsymbol{\theta}_{q(k)}^{d_{K,k}(t)}) - \nabla f(\boldsymbol{\theta}_{q(k)}^t) + \nabla f(\boldsymbol{\theta}_{q(k)}^t) \right\|_2^2 \right] \\ & = f(\boldsymbol{\theta}^t) - \gamma_t \sum_{k=1}^K \beta^{K-k} \left\| \nabla f(\boldsymbol{\theta}_{q(k)}^t) \right\|_2^2 - \gamma_t \mathbb{E} \left[\sum_{k=1}^K \beta^{K-k} \nabla f(\boldsymbol{\theta}_{q(k)}^t)^T \left(\nabla f_{\mathbf{x}_{d_{K,k}(t)}}(\boldsymbol{\theta}_{q(k)}^{d_{K,k}(t)}) - \nabla f(\boldsymbol{\theta}_{q(k)}^t) \right) \right] \\ & \quad + \frac{L\gamma_t^2}{2} \sum_{k=1}^K \beta^{K-k} \left\| \nabla f(\boldsymbol{\theta}_{q(k)}^t) \right\|_2^2 + \frac{L\gamma_t^2}{2} \mathbb{E} \sum_{k=1}^K \beta^{K-k} \left\| \nabla f_{\mathbf{x}_{d_{K,k}(t)}}(\boldsymbol{\theta}_{q(k)}^{d_{K,k}(t)}) - \nabla f(\boldsymbol{\theta}_{q(k)}^t) \right\|_2^2 \\ & \quad + L\gamma_t^2 \mathbb{E} \left[\sum_{k=1}^K \beta^{K-k} \nabla f(\boldsymbol{\theta}_{q(k)}^t)^T \left(\nabla f_{\mathbf{x}_{d_{K,k}(t)}}(\boldsymbol{\theta}_{q(k)}^{d_{K,k}(t)}) - \nabla f(\boldsymbol{\theta}_{q(k)}^t) \right) \right] \\ & = f(\boldsymbol{\theta}^t) - \left(\gamma_t - \frac{L\gamma_t^2}{2} \right) \sum_{k=1}^K \beta^{K-k} \left\| \nabla f(\boldsymbol{\theta}_{q(k)}^t) \right\|_2^2 + \tilde{Q}_1 + \tilde{Q}_2 \end{aligned} \quad (\text{b})$$

where the second inequality is due to $0 < \beta \leq 1$.

The \tilde{Q}_1 is bounded by

$$\begin{aligned}
\tilde{Q}_1 &= \frac{L\gamma_t^2}{2} \mathbb{E} \left[\sum_{k=1}^K \beta^{K-k} \left\| \nabla f_{\mathbf{x}_{d_{K,k}(t)}}(\boldsymbol{\theta}_{q(k)}^{d_{K,k}(t)}) - \nabla f(\boldsymbol{\theta}_{q(k)}^t) \right\|_2^2 \right] \\
&= \frac{L\gamma_t^2}{2} \mathbb{E} \left[\sum_{k=1}^K \beta^{K-k} \left\| \nabla f_{\mathbf{x}_{d_{K,k}(t)}}(\boldsymbol{\theta}_{q(k)}^{d_{K,k}(t)}) - \nabla f(\boldsymbol{\theta}_{q(k)}^{d_{K,k}(t)}) - \nabla f(\boldsymbol{\theta}_{q(k)}^t) + \nabla f(\boldsymbol{\theta}_{q(k)}^{d_{K,k}(t)}) \right\|_2^2 \right] \\
&\leq L\gamma_t^2 \mathbb{E} \left[\sum_{k=1}^K \beta^{K-k} \left\| \nabla f_{\mathbf{x}_{d_{K,k}(t)}}(\boldsymbol{\theta}_{q(k)}^{d_{K,k}(t)}) - \nabla f(\boldsymbol{\theta}_{q(k)}^{d_{K,k}(t)}) \right\|_2^2 \right] + L\gamma_t^2 \tilde{P}_1 \\
&= L\gamma_t^2 \sum_{k=1}^K \beta^{K-k} \mathbb{E} \left[\left\| \nabla f_{\mathbf{x}_{d_{K,k}(t)}}(\boldsymbol{\theta}_{q(k)}^{d_{K,k}(t)}) - \nabla f(\boldsymbol{\theta}_{q(k)}^{d_{K,k}(t)}) \right\|_2^2 \right] + L\gamma_t^2 \tilde{P}_1 \\
&\leq L\gamma_t^2 \sum_{k=1}^K \beta^{K-k} \mathbb{E} \left[\left\| \nabla f_{\mathbf{x}_{d_{K,k}(t)}}(\boldsymbol{\theta}_{q(k)}^{d_{K,k}(t)}) \right\|_2^2 \right] + L\gamma_t^2 \tilde{P}_1 \\
&\leq L\gamma_t^2 M \sum_{k=1}^K \beta^{K-k} + L\gamma_t^2 \tilde{P}_1 \\
&= L\gamma_t^2 M \frac{\beta^K - 1}{\beta - 1} + L\gamma_t^2 \tilde{P}_1
\end{aligned}$$

where the first inequality follows from $\|\mathbf{x} + \mathbf{y}\|_2^2 \leq 2\|\mathbf{x}\|_2^2 + 2\|\mathbf{y}\|_2^2$, the second one is from (3) and $\mathbb{E}[\|\epsilon - \mathbb{E}[\epsilon]\|_2^2] \leq \mathbb{E}[\|\epsilon\|_2^2] - \|\mathbb{E}[\epsilon]\|_2^2 \leq \mathbb{E}[\|\epsilon\|_2^2]$, the third one follows from Assumption 2, and the \tilde{P}_1 can be bounded by

$$\begin{aligned}
\tilde{P}_1 &= \sum_{k=1}^K \beta^{K-k} \left\| \nabla f(\boldsymbol{\theta}_{q(k)}^{d_{K,k}(t)}) - \nabla f(\boldsymbol{\theta}_{q(k)}^t) \right\|_2^2 \\
&\leq L^2 \sum_{k=1}^K \beta^{K-k} \left\| \boldsymbol{\theta}_{q(k)}^t - \boldsymbol{\theta}_{q(k)}^{d_{K,k}(t)} \right\|_2^2 \\
&= L^2 \sum_{k=1}^K \beta^{K-k} \left\| \sum_{j=\max\{0, d_{K,k}(t)\}}^{t-1} (\boldsymbol{\theta}_{q(k)}^{j+1} - \boldsymbol{\theta}_{q(k)}^j) \right\|_2^2 \\
&\leq L^2 \sum_{k=1}^K \beta^{K-k} \sum_{j=\max\{0, d_{K,k}(t)\}}^{t-1} \left\| \boldsymbol{\theta}_{q(k)}^{j+1} - \boldsymbol{\theta}_{q(k)}^j \right\|_2^2 \\
&= L^2 \sum_{k=1}^K \beta^{K-k} \sum_{j=\max\{0, d_{K,k}(t)\}}^{t-1} \gamma_j^2 \beta^{2(K-k)} \left\| \nabla f_{\mathbf{x}_{d_{K,k}(t)}}(\boldsymbol{\theta}_{q(k)}^{d_{K,k}(t)}) \right\|_2^2 \\
&\leq L^2 M \sum_{k=1}^K \beta^{3(K-k)} \sum_{j=\max\{0, d_{K,k}(t)\}}^{t-1} \gamma_j^2 \\
&\leq \gamma_t^2 L^2 M \sum_{k=1}^K \beta^{3(K-k)} (t - \max\{0, d_{K,k}(t)\})
\end{aligned}$$

with the first inequality coming from the Assumption 1.

On the other hand, The \tilde{Q}_2 is bounded by

$$\begin{aligned}
\tilde{Q}_2 &= -(\gamma_t - L\gamma_t^2) \mathbb{E} \left[\sum_{k=1}^K \beta^{K-k} \nabla f(\boldsymbol{\theta}_{q(k)}^t)^T \left(\nabla f_{\mathbf{x}_{d_{K,k}(t)}}(\boldsymbol{\theta}_{q(k)}^{d_{K,k}(t)}) - \nabla f(\boldsymbol{\theta}_{q(k)}^t) \right) \right] \\
&= -(\gamma_t - L\gamma_t^2) \sum_{k=1}^K \beta^{K-k} \nabla f(\boldsymbol{\theta}_{q(k)}^t)^T \left(\nabla f(\boldsymbol{\theta}_{q(k)}^{d_{K,k}(t)}) - \nabla f(\boldsymbol{\theta}_{q(k)}^t) \right) \\
&\leq \frac{\gamma_t - L\gamma_t^2}{2} \sum_{k=1}^K \beta^{K-k} \left\| \nabla f(\boldsymbol{\theta}_{q(k)}^t) \right\|_2^2 + \frac{\gamma_t - L\gamma_t^2}{2} \tilde{P}_1
\end{aligned}$$

where the second equality follows by the unbiased gradient using SGD, the inequality comes from $\pm \mathbf{x}^T \mathbf{y} \leq \frac{1}{2} \|\mathbf{x}\|_2^2 + \frac{1}{2} \|\mathbf{y}\|_2^2$.

By substituting \tilde{Q}_1 and \tilde{Q}_2 into (b), the inequality is rewritten as

$$\begin{aligned}
\mathbb{E} \left[f(\boldsymbol{\theta}^{t+1}) \right] &\leq f(\boldsymbol{\theta}^t) - \left(\gamma_t - \frac{L\gamma_t^2}{2} \right) \sum_{k=1}^K \beta^{K-k} \left\| \nabla f(\boldsymbol{\theta}_{q(k)}^t) \right\|_2^2 \\
&\quad + \frac{\gamma_t - L\gamma_t^2}{2} \sum_{k=1}^K \beta^{K-k} \left\| \nabla f(\boldsymbol{\theta}_{q(k)}^t) \right\|_2^2 + \frac{\gamma_t - L\gamma_t^2}{2} \tilde{P}_1 + L\gamma_t^2 M \frac{\beta^K - 1}{\beta - 1} + L\gamma_t^2 \tilde{P}_1 \\
&\leq f(\boldsymbol{\theta}^t) - \frac{\gamma_t}{2} \sum_{k=1}^K \beta^{K-k} \left\| \nabla f(\boldsymbol{\theta}_{q(k)}^t) \right\|_2^2 + \frac{\gamma_t + L\gamma_t^2}{2} \gamma_t^2 L^2 M \sum_{k=1}^K \beta^{3(K-k)} (t - \max\{0, d_{K,k}(t)\}) \\
&\quad + L\gamma_t^2 M \frac{\beta^K - 1}{\beta - 1} \\
&= f(\boldsymbol{\theta}^t) - \frac{\gamma_t}{2} \sum_{k=1}^K \beta^{K-k} \left\| \nabla f(\boldsymbol{\theta}_{q(k)}^t) \right\|_2^2 \\
&\quad + \gamma_t^2 \left(LM \frac{\beta^K - 1}{\beta - 1} + \frac{\gamma_t + L\gamma_t^2}{2} L^2 M \sum_{k=1}^K \beta^{3(K-k)} (t - \max\{0, d_{K,k}(t)\}) \right) \\
&\leq f(\boldsymbol{\theta}^t) - \frac{\gamma_t}{2} \sum_{k=1}^K \beta^{K-k} \left\| \nabla f(\boldsymbol{\theta}_{q(k)}^t) \right\|_2^2 \\
&\quad + \gamma_t^2 \left(LM \frac{\beta^K - 1}{\beta - 1} + LM \sum_{k=1}^K \beta^{3(K-k)} (t - \max\{0, d_{K,k}(t)\}) \right)
\end{aligned}$$

where the last inequality follows from $L\gamma_t \leq 1$ such that $\frac{\gamma_t + L\gamma_t^2}{2} L \leq 1$. \square